This article has been accepted for publication in a future issue of this journal, but has not been fully edited. Content may change prior to final publication. Citation information: DOI 10.1109/TSTE.2018.2885946, IEEE Transactions on Sustainable Energy

3D Layout Optimization of Wind Turbines Considering Fatigue Distribution

Ling-ling Huang, *Member, IEEE*, Hua Tang, Kai-hua Zhang, Yang Fu, Yang Liu

***Abstract*—As wind resources and land resources become increasingly strained with the rapid expansion of wind energy, the problem of getting a better micro-sitting of wind turbines has gained more and more concerns in the wind industry. A methodology of three-dimension layout of wind turbines (WTs) is proposed in this paper to optimize the horizontal layout and vertical hub height simultaneously. New development of low speed WT technology and influences of micro-sitting of WTs to their O&M costs are considered for the first time. A nested loop consisting of a Harmony Search Algorithm (HS) based layout optimization and a Sorting Genetic Algorithm-II (NSGA-II) based turbine selection is also presented to deal with the multi-objective functions. In the optimization process, a polar coordinate transformation based wake effect model is conducted to simplify the wake effect calculations among the multi wind turbines with different hub height and rotor diameters when the wind direction changes. A 100MW wind farm case is discussed to illustrate the flexibility and performance improvements of the proposed methodology.**

***Index Terms*—Layout optimization, turbine selection, fatigue distribution, wake effect.**

I. Introduction

Wind energy, as one of the most common and mature renewable energy, has made significant development in recent ten years. According to GWEC, the global installed capacity of wind power has achieved 539.1GW by the end of 2017 and will reach 840GW by 2020. The significant installed capacity of wind energy makes the wind turbines (WTs) a common sight almost all around the world. With the rapid expansion of wind energy, the scarcity of good wind resources and land resources becomes increasingly intensive. Meanwhile, mass production of WTs leads to a brutal competition between WT manufacturers and wind farm owners. Power generations of neighboring wind farms are fiercely contested almost every quarter or even every week. As wind farm micro-sitting has significant effects on the power generation and wind farm investment, optimization of WTs selections and layout has gained more and more attention and is now a critical problem in wind farm planning[1,2].

Many research works have been done on wind farm micro-sitting. For WT selections, Jangamshetti *et al*. first proposed a resource matching coefficient in [3] as a technical selection index. Doddamani *et al*. [4] presented a simplified WT cost model for the economic-based WT selection. After comparing four different economic indexes in [5], Li *et al*. pointed out that the two most important parameters of choosing WTs are the rated capacity and the rated wind speed. Shafiqur *et al* [6] provided a multi-criteria WT selection strategy to deal with the conflicts between the technical requirement and economic restrictions. For WTs layout, as wake effect accounted for 5~15% power losses of the wind farm [7], many layout optimizations have been proposed based on the strategy of reducing wake effect. Herbert-Acero *et al*. [8] lined up the WTs in the main wind direction and optimized positions by using both Simulated Annealing and Genetic Algorithm (GA). And then, some researchers [9-11] extended the layout optimizations from a line to a plane. The site of the wind farm was gridded into many small squares, and then different algorithms were proposed to find the optimal locations to achieve the maximal power generation or the minimal levelized cost of energy (LCOE). The WTs were assumed to be located at the central point of each grid, so the results highly depended on the size of the grid. Souma *et al*. developed an unrestricted wind farm layout optimization (UWFLO) model [12] to eliminate turbine locating restrictions in a discrete grid. Some other studies also improved the power generations by adjusting the hub height of WTs [13,14]. Moreover, with the positions of WTs settled, some meticulous control strategies of WTs in the wind farm have been presented for reducing the wake effect and capturing more wind power [15-17].

However, in most of these researches, the WTs in a wind farm are supposed to be the same type. The development of low wind speed turbine techniques provides more choices of WTs with the same capacity. For example, NORDEX provides four kinds of 1.5MW WTs with different diameters that have different wind capture performances and different prices. Mixed utilization of WTs with different rotor diameters is seldom considered. Moreover, the existing researches of wind farm micro-sitting ignore the influences of WTs layout to their

This work was supported by National Natural Science Foundation of China (51707112), Shanghai Engineering Research Center of Green Energy Grid-Connected Technology (13DZ2251900), and " Electrical Engineering" Shanghai class II Plateau Discipline.(Corresponding author: Yang Fu.)

L. Huang is with Shanghai University of Electric Power, Shanghai 200444, China (e-mail: linglinghuang82@gmail.com).

H. Tang is with Weifang Power Supply Company, State Grid Shandong Electric Power Company, Weifang 261021, China (e-mail: tanghua0536@163.com).

K. Zhang is with Green Environmental Protection Energy Co., Ltd., Shanghai, 200433,China (e-mail: zhangkhk@sina.com).

Y. Fu and Y. Liu are with Shanghai University of Electric Power, Shanghai,200090,China(e-mail:mfudong@126.com;liuyang_ssun@163.com

This article has been accepted for publication in a future issue of this journal, but has not been fully edited. Content may change prior to final publication. Citation information: DOI 10.1109/TSTE.2018.2885946, IEEE Transactions on Sustainable Energy

operation and maintenance (O&M). Laboring intensities of WTs in a wind farm are highly inhomogeneous. According to [18], WTs in the upstream of the main wind direction are more fatigued than the others and require 1.5 times more frequent maintenance.

This paper presents a three-dimension (3D) layout optimization of WTs both considering the horizontal layout and the vertical height determined by the rotor diameters. The fatigue damages of every WT in the wind farm caused by different WT selections and layouts are also considered. And a simplified maintenance cost model related to the fatigue distribution is proposed. In order to achieve the minimal LCOE and the most uniform fatigue distribution, a nested algorithm is proposed in this paper, while Harmony Search Algorithm (HS) is introduced to solve the WT layout problem and Non-dominated Sorting Genetic Algorithm-II (NSGA-II) is used to optimize the bi-objective WT diameter selection.

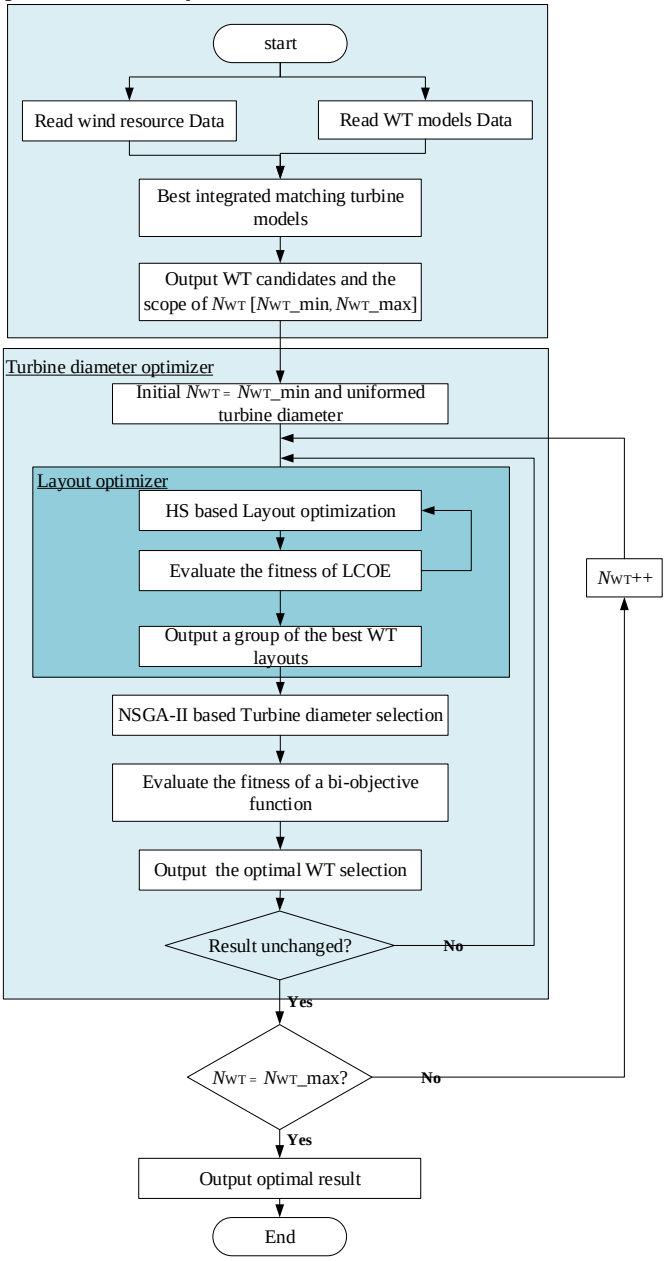

Figure 1. A procedure of 3D layout optimization methodology

II. Modeling of 3D Layout Optimizations

Wind farm micro-sitting mainly includes the selections of WT unit capacity, turbine diameters, and locations. As the capacity of the WT is mainly determined by the wind conditions and power curves of the WTs, there is a limit space for WT selection optimization.

Depending on turbine diameters, the locations of WTs downstream are changed and their turbine diameters are also influenced by the shadows of the upstream WTs. Short blades upstream capture less wind energy and the downstream WTs will be less influenced by the wake effect while long blades upstream captures more wind energy and leaves less energy for the downstream turbines. With the overall balance of wind energy, there is an optimization problem of selecting turbine diameters upstream and downstream. And there is also a tradeoff between the power losses caused by wake effect and the space the upstream and downstream WTs occupied.

Moreover, a longer running and more power captures of a WT also represent a more fatigued state and a higher possibility of being failed. Spread the labors equally will help to keep the healthy state of WTs and make synchronous maintenance of several WTs possible. So, labor intensity should be handled together with WT selections and layout.

To do this, this paper proposes a methodology consisting of two parts: a primary selection and two nested optimizers performed repeatedly, as depicted in Fig.1. Firstly, the primary selection provides the candidate WT types with the best wind energy capturing performance under the given wind resource. Then, according to the size of the wind farm or the requirement of the wind farm owners, the maximal and minimal number of WTs in the wind farm will be calculated. The nested loop is composed of 'Layout Optimizer' and 'Turbine diameter Optimizer'. The inner loop 'Layout Optimizer' is to provide a group of WT layouts with the minimal LCOE, while the outer loop 'Turbine diameter Optimizer' is to select the best WT diameters to achieve the minimal LCOE and minimal fatigue standard deviation at the same time. The nested loop will stop until the optimal result unchanged with the given N_{WT}. An exhaustive approach is utilized for different N_{WT}. The entire procedure is illustrated in Fig.1.

A. The Preliminary WT Selections

There are several WT types in the market with different performances and prices. The primary WT selection picks out the candidate WT types with the best wind capturing performances as well as cost-effective.To do this, an integrated index λ is defined as:

$$\lambda = \frac{\mu}{\sigma} \tag{1}$$

where, σ represents the cost of the WT, and μ represents the matching degree of the WT and the wind resources.

The cost of WT can be simplified as a function of the rated power (P_r) and the hub height of the WT (H) [19], which is:

$$\sigma = \frac{0.0003P_r^2 + 0.37P_r + 3.8H - 140}{P_r} \tag{2}$$

The power curve of a WT demonstrates its wind energy

This article has been accepted for publication in a future issue of this journal, but has not been fully edited. Content may change prior to final publication. Citation information: DOI 10.1109/TSTE.2018.2885946, IEEE Transactions on Sustainable Energy

capturing performance clearly, as shown in Fig.2. Besides the rated power, there are three other main parameters determining the wind energy capturing performance. They are cut-in wind speed v_{in}, cut-out wind speed v_{out}, and rated wind speed v_{rate}. Generally, wind farms with low wind speed resources prefer WTs with low v_{in}, while wind farms with high wind speed resources prefer WTs with low v_{rate}. In order to calculate the matching degree of the WT and the wind resources quantitatively, a matching degree μ is shown in (3) [19].

$$\mu = \frac{1}{4(v_{in}+v_{rate})}\left[\xi(v_{in})+3\xi\left(\frac{v_{in}+2v_{rate}}{3}\right)+3\xi\left(\frac{v_{rate}+2v_{in}}{3}\right)+\xi(v_{rate})\right]-\frac{\xi(v_{out})}{v_{out}} \tag{3}$$

where, $\xi(v)$ is a function. It can be calculated as

$$\xi(v) = v\cdot\exp\left[-\left(\frac{v}{c}\right)^{k}\right] \tag{4}$$

where, v represents the wind speed which may be v_{in}, v_{rate}, v_{out} or the expressions inside the brackets in (3). c and k are the scale parameter and shape parameter in Weibull distribution respectively which describes the wind resource characteristic [20].

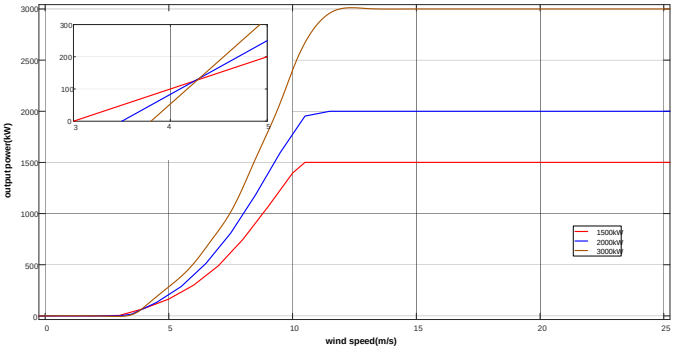

Figure 2. Power curve of WTs with different rated power

As the types of WT in the market are limited, selections of the candidate WTs can be taken by an exhaustive approach. Considering that the number of candidate WT types should be the more the better for the fatigue distribution homogenization, but the less the better for the simplicity of spare part management, the number of candidate WT types may be chosen based on the unified management of several wind farms owned by the wind farm owners.

The number of WTs in the given wind farm should satisfy the smallest distance restriction between any two WTs for the safety concerns, which is usually 4 times of the blade diameter [21]. Supposing R_{min} is the shortest rotor diameter of the candidate WTs, the maximal and minimal number of WTs in the given wind farm can be calculated as:

$$\begin{cases} N_{WT\_max} = round\left(\dfrac{S}{\alpha_r \pi (2R_{min})^2}\right) \\ N_{WT\_min} = 1 \end{cases} \tag{5}$$

where, N_{WT_max} and N_{WT_min} are the maxmimal and minimal number of WTs respectively. S is the area of the given wind farm. α_r is the safety coefficient of the smallest distance restrictions. Round is a mathematical symbol.

Sometimes the capacity of the wind farm is settled, the optimization is carried out with the same installed capacity.Then the maxmimal and minimal number of WTs in the given wind farm will be determined by the unit capacity of the candidate WT, which is

$$\begin{cases} N_{WT\_max} = round\left(\dfrac{P_{WF}}{P_{min}}\right) \\ N_{WT\_min} = round\left(\dfrac{P_{WF}}{P_{max}}\right) \end{cases} \tag{6}$$

where, P_{WF} is the capacity of the wind farm, P_{min} and P_{max} are the maxmimal and minimal capacity of the candidate WTs respectively.

B. Optimization Models of the Nested Loop

The nested optimizations aim to optimize the WT selections and the layout simultaneously. In order to demonstrate the influences of micro-sitting of WTs to their fatigue damages, a fatigue standard deviation is defined to achieve the most uniform fatigue distribution. The objectives will be:

$$\begin{cases} \min F(N_{WT}, x_i, y_i, D_i, H_i) = [f_1, f_2]^T \\ f_1 = \min(LCOE) = \min\left(\dfrac{C_{cost}}{P_{total}}\right) \\ f_2 = \min\sqrt{\dfrac{1}{N_{WT}}\sum_{i=1}^{N_{WT}}\left(F_i - F_{group}\right)^2} \\ s.t.\ D_i \in D_f, H_i \in H_f, (x_i, y_i) \subset S \\ \sqrt{(x_i-x_j)^2+(y_i-y_j)^2} \geq 4D_i, i \neq j \in [1, n] \end{cases} \tag{7}$$

where, N_{WT} is the number of WTs in the wind farm, x_i and y_i are the coordinates of the i^{th} WT, D_i and H_i are the rotor diameter and hub height of the i^{th} WT respectively. f_1 and f_2 are two objective functions representing LCOE and fatigue standard deviation respectively. C_{cost} is the life cycle cost (LCC), P_{total} is the total power generations during the life cycle, F_i is the turbine fatigue of the i^{th} WT, F_{group} is the average fatigue of all WTs in the wind farm. Rotor diameters and hub height of the WTs should belong to the alternative sets D_f and H_f. S is the wind farm area. Besides, the last inequality in (5) is the smallest distance restrictions between any two WTs.

C. Fatigue Damages of WTs

Causes of turbine fatigues mainly consist of two parts: working fatigues accumulated during power generations and the fatigues caused by the effect of turbulence. Researchers in [22] defined a fatigue coefficient to describe these comprehensive fatigue damages of a WT by analyzing the relationship between the fatigues and power outputs. The fatigue coefficient of the ith WT F_i can be expressed as

$$F_i(t) = (1+\gamma)\frac{\int_0^t P_i(\tau)d\tau}{P_{rate}T_{life}(1+C_{rep})} \tag{8}$$

where, γ is a ratio describing the effect of turbulence, which is generally 5% to 15%. $P_i(t)$ is the power output of WT i at the

This article has been accepted for publication in a future issue of this journal, but has not been fully edited. Content may change prior to final publication. Citation information: DOI 10.1109/TSTE.2018.2885946, IEEE Transactions on Sustainable Energy

moment *t*. T_{life} is the life cycle of WTs, and C_{rep} is a maintenance compensation factor which is an empirical constant.

Fatigue damage is an important issue relating to the maintenance cost. According to [23], it is expected that at least half of all mechanical failures are due to fatigues. In order to get the relations between WT fatigue and the maintenance cost, two maintenance is considered including preventive maintenance and corrective replacement. It fits engineering reality of big mechanical components of WTs, like gearboxes and shafts. To simplify the calculation, preventive maintenance is supposed to be taken periodically. The maintenance period T_{PM} is usually half a year in a lot of wind farms [24].

$$p_{PM} = \frac{1}{T_{PM}} \tag{9}$$

where, p_{PM} is the frequency of preventive maintenance.

An age reduction factor α_m is considered to evaluate the effect of every preventive maintenance.

$$F_{after} = \alpha_m F_{before} \tag{10}$$

where, F_{before} and F_{after} are the fatigues before and after the preventive maintenance respectively.

When the fatigue reaches a certain level F_{fault}, a corrective replacement will be taken place. So, for a wind farm installed with N_{WT} WTs, the frequency of corrective replacement will be the numbers of WTs whose fatigue reaches the level F_{fault} during every preventive maintenance period, which can be expressed as:

$$p_{CM} = \frac{\sum_{m=1}^{\infty}\sum_{i=1}^{N_{WT}} M\left\{F_i(t) \geq F_{fault}, t \in T_{PM(m)}\right\}}{\sum_{m=1}^{\infty} T_{PM(m)}} \tag{11}$$

where, p_{CM} is the frequency of corrective replacement. *m* is the number of maintenance period. $T_{PM(m)}$ is the *m*-th preventive maintenance period.

When a replacement is taken place, the component will be brand new. So the fatigue value after the corrective replacement will be:

$$F_{after} = 0 \tag{12}$$

D. LCC Modeling

The LCC of a wind farm is determined by the initial investment and O&M costs. The initial investment includes the turbine costs and the relevant costs of constructions. For the WTs with the same rated power, this initial investment is mainly determined by the hub height *H* and rotor diameters *D*. The O&M costs during the life cycle should be converted to a present value. Thus, the LCC of a wind farm can be expressed as:

$$C_{\text{cost}} = \sum_{i=1}^{N_{WT}} (C_{WT}(D_i, H_i) + C_{cons}(D_i, H_i) + I_v C_{\text{main}} + C) \tag{13}$$

where, C_{WT} and C_{cons} represent the turbine cost and the variable part of the construction cost respectively. They are both related to *D* and *H*. The fixed part of the turbine and construction is defined as a constant *C*. I_v is the discount factor. And C_{main} represents the O&M cost which is determined by the frequencies of corrective replacement and preventive maintenance. It can be calculated as

$$C_{\text{main}} = T_{life}(p_{CM} C_{CM} + p_{PM} C_{PM}) \tag{14}$$

where, C_{CM} and C_{PM} represent the costs of corrective replacement and preventive maintenance respectively.

E. Wake Effect

When the wind flows through a WT, kinetic energy of the wind is partly absorbed by the turbine blades and the rest will be massively separated weakening the wind energy for the downstream WT. This wake effect highly depends on the shadow area between the upstream and downstream WTs, as shown in Fig.3.

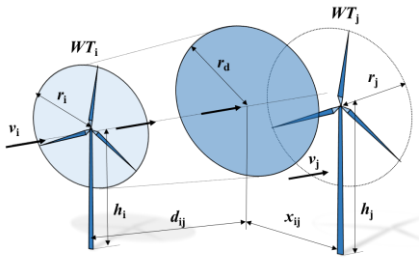

Figure 3. Wake effect between wind turbine with different hub height and diameter

The dynamic behavior of the wake effect in reality is very complicated, and a lot of work has been done on the modeling. In this research, the wind farm is planned for the entire life cycle, the consideration of the steady-state of the wake effect is preferred [25]. As the Jensen's wake loss model provides a simple but reasonable description of the steady-state of the wake effect [26], it has been widely used in WT layout optimizations [7,27]. Thus it is considered in this research.

To calculate the wake effect in turbines with different hub height, the wind velocity difference caused by height should be taken into consideration. For a known measured wind speed v_i at a height h_i, the wind speed v_j at a height h_j can be expressed as (14), where α represents surface friction coefficient [28].

$$\frac{v_j}{v_i} = \left(\frac{h_j}{h_i}\right)^{\alpha} \tag{14}$$

According to multiple wake model [29], the downstream wind speed v_i' at a distance d_{ij} in height h_i is:

$$v_i' = v_i\left[1 - \sum_{i=1}^{n}\left(1-\sqrt{1-C_T}\right)\left(\frac{r_i}{r_d}\right)^2 \frac{A_s}{A_j}\right] \tag{15}$$

Thus, the wake model which is available for various hub height and rotor diameter has been improved by combining equation (14) and (15):

$$v_j = v_i'\left(\frac{h_j}{h_i}\right)^{\alpha} = v_i\left[1 - \sum_{i=1}^{n}\left(1-\sqrt{1-C_T}\right)\left(\frac{r_j}{r_d}\right)^2 \frac{A_s}{A_j}\right]\left(\frac{h_j}{h_i}\right)^{\alpha} \tag{16}$$

where, C_T is the turbine thrust coefficient, A_j and A_s represent rotor swap area and the shadowed area of the downstream WT respectively. r_j is the radius of the swap area. And r_d is the radius of the shadowed area, which can be calculated by the

This article has been accepted for publication in a future issue of this journal, but has not been fully edited. Content may change prior to final publication. Citation information: DOI 10.1109/TSTE.2018.2885946, IEEE Transactions on Sustainable Energy

longitudinal distance (d_{ij}) of the two WTs and the wake expand coefficient (k_w), which can be expressed as

$$r_d = r_i + k_w d_{ij} \tag{17}$$

For a wind farm, the shadow areas between the upstream and downstream WTs depend on their hub height, rotor diameters and the changes of wind directions. A_s is improved in this paper based on [28] to deal with the different hub height and rotor diameters, which is:

$$\begin{aligned} A_s = {} & r_d^2 \cos^{-1}\left(\frac{r_d^2 + x_{ij}^2 + \Delta h^2 - r_j^2}{2r_d\sqrt{\Delta h^2 + x_{ij}^2}}\right) + r_j^2 \cos^{-1}\left(\frac{r_j^2 + x_{ij}^2 + \Delta h^2 - r_d^2}{2r_j\sqrt{\Delta h^2 + x_{ij}^2}}\right) \\ & - r_d\sqrt{\Delta h^2 + x_{ij}^2} \cdot \sin\left(\arccos\left(\frac{r_d^2 + x_{ij}^2 + \Delta h^2 - r_j^2}{2r_d\sqrt{\Delta h^2 + x_{ij}^2}}\right)\right) \end{aligned} \tag{18}$$

where, x_{ij} and Δh represent the distance and hub height difference between the upstream and downstream WTs.

When the wind direction changes, the positions of upstream and downstream WTs may be changed. To deal with this problem, literature [7] constructed a look-up table to ascertain whether a WT is the upstream or the downstream one, then calculated the latitudinal and longitudinal distances under the given wind direction. Small changes in the wind direction may be not noticed in the finite data provided by the look-up table. In this paper, a simplified method for calculating the shadow area with varied wind direction is proposed by introducing the polar transformation as shown in Fig.4.

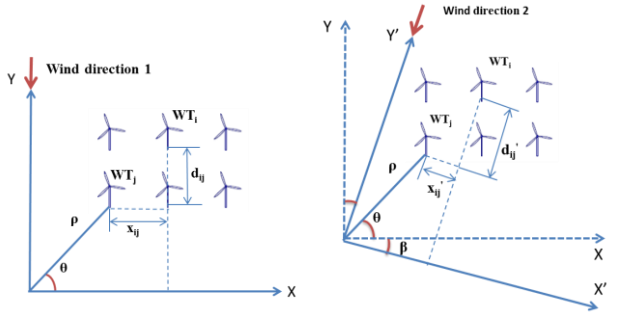

Figure 4. Wind turbine relative position in different wind direction

Supposing there are two WTs: WT_i and WT_j. The coordinates of them are (x_i,y_i) and (x_j,y_j), polar coordinates are (ρ_i,θ_i) and (ρ_j,θ_j). Therefore, latitudinal and longitudinal distance x_{ij}、d_{ij} can be expressed as:

$$\begin{cases} x_{ij} = x_i - x_j = \rho_i \cos\theta_i - \rho_j \cos\theta_j \\ d_{ij} = y_i - y_j = \rho_i \sin\theta_i - \rho_j \sin\theta_j \end{cases} \tag{19}$$

When wind direction turns β degrees in Y direction (from wind direction 1 to wind direction 2 in the first quadrant as illustrated in Fig.4), the new latitudinal and longitudinal distance can be calculated by the inverse transformation.

$$\begin{cases} x_{ij}^{'} = \sqrt{x_i^2 + y_i^2}\cos(\tan^{-1}\frac{y_i}{x_i} + \beta) - \sqrt{x_j^2 + y_j^2}\cos(\tan^{-1}\frac{y_j}{x_j} + \beta) \\ d_{ij}^{'} = \sqrt{x_i^2 + y_i^2}\sin(\tan^{-1}\frac{y_i}{x_i} + \beta) - \sqrt{x_j^2 + y_j^2}\sin(\tan^{-1}\frac{y_j}{x_j} + \beta) \end{cases} \tag{20}$$

With (18) and (20), the shadow area as well as WT location can be easily obtained accurately.

F. Energy Production Calculation

The expected energy production of the wind farm is mainly determined by the local wind resources, which are usually depicted as wind speed and wind direction distribution. Normally, the Weibull distribution and rose diagram, as shown in Fig.5 and Fig.6, are introduced to demonstrate the distribution of wind speed and wind directions. Supposing that there are q wind speeds and p wind directions in Fig.5 and Fig.6, the energy production P_{total}, which is the sum of each power generations of the N_{WT} turbines, can be calculated as

$$P_{total} = T_{life}\sum_{i=1}^{N_{WT}}\sum_{v=v_1}^{v_q}\sum_{\beta=\beta_1}^{\beta_p}\left(P_i(\beta,v)\cdot 8760 g(v) g(\beta)\right) \tag{21}$$

where, $P_i(\beta,v)$ is the output power of i^{th} WT at a specific wind direction β and wind speed v. $g(v)$ and $g(\beta)$ are the annual frequency of wind speed and wind direction respectively.

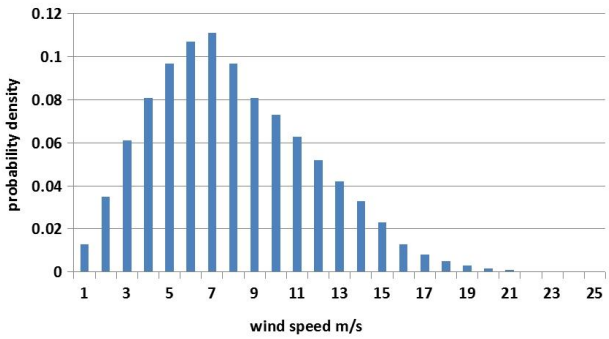

Figure 5. Probability density of annual mean wind speed

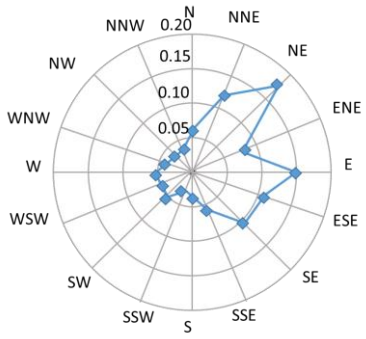

Figure 6. Frequencies of annual wind direction

It must be emphasized that for WTs with different rotor diameters but the same rated capacity, v_{in}, v_{out} and v_{rated} are very close as shown in Fig.7. To distinguish the energy capturing performance, method of interpolation can be introduced to get the output power at different wind speed based on fitting power curves provide by WT manufacturers.

This article has been accepted for publication in a future issue of this journal, but has not been fully edited. Content may change prior to final publication. Citation information: DOI 10.1109/TSTE.2018.2885946, IEEE Transactions on Sustainable Energy

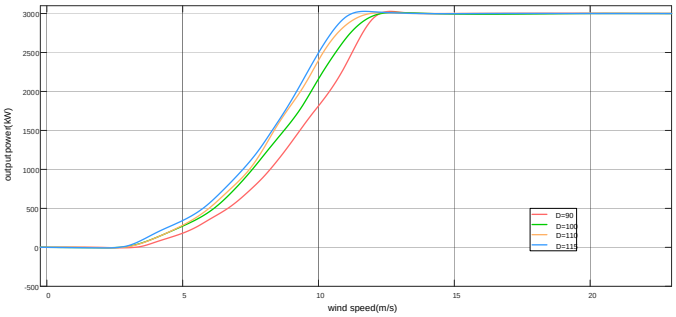

Figure 7. Power curve of WTs with same rated power

III. Optimization Algorithms

By analyzing the 3D layout optimization model, it can be found that it is a multi-objective problem with multi discrete variables. This paper introduced two intelligent algorithms to solve this problem. In the nested loop, HS is introduced to find a group of the optimal WT layouts while NSGA-II is introduced to find the best diameters of each WT for a multi-objective optimization of both lowest LOCE and smallest fatigue standard deviation.

A. HS based horizontal layout optimization

HS is a metaheuristic algorithm imitating the improvisation process of music players developed by Zong Woo Geem *et al*. [30]. The advantage of HS is that it has a simpler searching process and a stronger global searching ability. Comparing with GA, HS considers all the existing vectors rather than considering only two parents [31].

For a wind farm with N_{WT} WTs, each WT has a position (x_i, y_i). The combination of N_{WT} positions is a layout solution $\{x_1, \dots, x_{NWT}, y_1, \dots, y_{NWT}\}$. f is the fitness representing LCOE here which can be calculated by (7).

Firstly, a group of layout solutions are generated randomly and the fitnesses are calculated correspondingly. Then, a harmony memory (HM) is generated by combining the layout solution and the fitness. An example of a HM is presented in (22).

$$HM = \begin{bmatrix} x_1^1 \cdots x_{N_{WT}}^1 & y_1^1 \cdots y_{N_{WT}}^1 & f^1 \\ x_1^2 \cdots x_{N_{WT}}^2 & y_1^2 \cdots y_{N_{WT}}^2 & f^2 \\ \vdots \cdots \vdots & \vdots \cdots \vdots & \vdots \\ x_1^s \cdots x_{N_{WT}}^s & y_1^s \cdots y_{N_{WT}}^s & f^s \end{bmatrix} \tag{22}$$

where, s represents the size of the initial solutions.

After that, the improvisation is carried out to generate a new harmony. There are two ways: the one is to select a harmony from the existed HM and get a new harmony by making a minor adjustment. The other is to create a harmony randomly within the range of variable x_i and y_i. The new harmony will be compared with the worst one in the existed HM. During the HM update, the worst solution is replaced by the new one. HS will be continuously carried on until it reaches the maximum iteration.

B. NSGA-II based WTs selections

The optimal problem with more than one objective is called multi-objective optimization (MOP) [32]. The difficulty in solving MOP is that the sub-goals might be contradictory to each other. The improvement of one objective function may cause the decrease in another. A popular solution to the MOP problem is to turn it to a single objective problem by weighing summation. But it is difficult to choose the perfect weighed coefficients. NSGA-II is one of the most popular multi-objective optimization algorithms. It is a fast non-dominated sorting approach with a fast crowded distance estimation procedure and a simple crowded comparison operator [33].

The population initialization in this paper can be realized with binary encoding. The diameter of each WT is defined as the optimization variable. For each WT, an X-bit binary code is created to describe the selected WT types. For example, if there are four types of blades, the binary encoding can be 00, 01, 10 and 11. Thus, for a wind farm with N_{WT} WTs, the chromosome length will be $N_{WT} \times X$. NSGA-II has roughly the same process of traditional GA, which can be found in [34,35]. As the algorithm is not the key point in this paper, only the differences between NSGA-II and traditional GA are presented here. The primary difference is in the process of the individual selection, which contains non-dominated sort and crowding distance rank in NSGA-II. In non-dominated sort, a combined set is created consisting of the initial population and the generated offspring. Each individual is calculated in terms of two fitness. The noninferior solutions are taken out and put into a Pareto set. By repeating the selections of noninferior solutions, a group of Pareto sets are generated until all the individuals are sorted. In the process of crowding distance ranking, the differences of finesses between the neighboring individuals in the same Pareto set are calculated and ranked from the largest to the smallest. Then, the new population will be obtained by selecting the best individuals. The optimization continues with the new generation until it meets the convergence conditions.

IV. Case Study

For the test system of case study, a quadrangle wind farm with total area of 18.75 km^2 is shown in Fig.8 and the total installed capacity is expected to be 100 MW. The air density in this area is 1.241 kg/m^3, average wind speed in 70m is 6.77m/s. And the wind speed is supposed to fit the Weibull distribution while the scale parameter c=7.5, and the shape parameter k=1.83. The wind shear exponent α=0.163, and the probability density of each wind speed calculated by Weibull parameter is shown in Fig.5 the wind rose diagram is shown in Fig.6.

Wind conditions in different height can be calculated according to the power law of wind shear, as shown in Tab.I.

This article has been accepted for publication in a future issue of this journal, but has not been fully edited. Content may change prior to final publication. Citation information: DOI 10.1109/TSTE.2018.2885946, IEEE Transactions on Sustainable Energy

TABLE I
THE AVERAGE WIND SPEED AND WEIBULL PARAMETER IN DIFFERENT HEIGHT

H (m)	Average wind speed (M/S)	Scale parameter c	Shape parameter k
50	6.41	6.8	1.76
60	6.60	7.2	1.80
70	6.77	7.5	1.83
80	6.92	7.7	1.85
90	7.05	8.0	1.87
100	7.18	8.2	1.89
110	7.29	8.4	1.9

A. *Preliminary WT Type Selection*

The candidate WTs are shown in Tab.II which are the mainstream onshore WTs in the market. The main parameters (including P_r, v_{in}, v_r, v_{out}, H, D) are listed in the first seven columns of Tab.II. According to (1-4), the performance indexes μ, σ and λ can be calculated, as depicted in the last three columns in Tab.II.

TABLE II.
WT DATA AND CALCULATED EVALUATION INDEX OF ALTERNATIVE TYPES

WT	P_r kW	v_{in} m/s	v_r m/s	v_{out} m/s	H/D m	μ	σ	λ
1	850	4	16	25	50/52	0.1449	0.6838	0.2119
2	1500	3.5	14	25	70/77	0.2426	0.9040	0.2683
3	1500	3	13	25	70/70	0.2183	0.9040	0.2415
4	1500	3	12.5	25	70/77	0.2308	0.9040	0.2554
5	1500	3	12	25	80/82	0.2597	0.9293	0.2795
6	1500	3	11	20	80/88	0.2747	0.9293	0.2957
7	2000	4	13.5	25	60/80	0.2281	1.0140	0.2249
8	2000	4	12.5	25	70/87	0.2820	1.0330	0.2730
9	2000	3	12.3	25	70/90	0.3136	1.0330	0.3036
10	2000	3.5	13	25	80/80	0.2897	1.0520	0.2754
11	2000	4	16	25	70/80	0.1797	1.0330	0.1739
12	2300	4.5	13.5	25	80/81	0.2488	1.1313	0.2200
13	2300	4	13.5	25	80/93	0.2607	1.1313	0.2305
14	2500	3.5	12	25	80/97	0.3287	1.1856	0.2773
15	2500	3.5	12.5	25	70/90	0.2943	1.1704	0.2515
16	2500	3.5	11	25	90/103	0.3960	1.2008	0.3298
17	3000	3	13	25	80/90	0.4201	1.3247	0.3172
18	3000	3	12.5	25	90/100	0.4522	1.3373	0.3382
19	3000	3	12	25	100/110	0.4947	1.3500	0.3665
20	3000	3.5	11.5	25	110/115	0.4960	1.3627	0.3640

From the last three columns of Tab.II, it can be noted that the last five types including WT16-WT20 are with the maximal λ, which means these five WTs are the most cost-effective options in this case. WT16-WT20 can be the candidates for the following optimizations. If the WTs in the wind farm are expected to be with the same capacity, four WTs including WT17-WT20 can be the candidates. In order to illustrate the application of the low speed WTs and to compare the results of different method, this paper picks up the WTs with the same capacity. So the optimal candidate WTs in the wind farm will be WT17-WT20 with 3MW each. And N_{WT} = 34. The detailed information of the selected turbines is shown in Tab.III.

TABLE III.
THE DETAILED INFORMATION OF TURBINE AND CONSTRUCTION COST ($\times 10^3$) OF 4 CANDIDATE WTS

WT model		WT17	WT18	WT19	WT20
Turbine cost relating to D and H	Blade cost	101.8	136.4	177.7	201.3
	Pitch drive cost	75.1	99.3	127.9	143.9
	Rotor shaft cost	29.0	42.1	58.9	68.9
	Yaw drive cost	42.0	57.4	76.2	86.9
	Nacelle cost	78.1	95.9	115.6	126.1
	Tower cost	301.1	419.1	564.2	678.8
Construction cost relating to D and H	Base cost	61.0	69.7	78.5	84.6
	Installation cost	66.1	85.9	108.7	128.1
Fixed cost	/	1023.8			

B. *Impact of Horizontal Layout*

In order to demonstrate the impacts of horizontal layout of WTs, the WTs in the wind farm are supposed to be the same type. WT 19 in Tab.II is picked here. Traditionally, to simplify the WT layout, the WTs in the wind farm are settled in wonderful arrays, as shown in Fig.8 (I). The dots in the figure represent the WTs. WTs with the same type and the same number are resettled by optimizing their horizontal positions. Lower LCOE is achieved by the layout optimizer in Fig.1. The optimized result is displayed in Fig.8 (II).

Comparing these two different layouts in Fig.8 (I) and (II), it can be found that: 1) Changing the horizontal layout of WTs in a wind farm may help to improve the power generation. It has a 5.7% increase here. 2) WTs layout should take full advantages of the landform and the wind direction distribution. In this example, the shape of this wind farm is roughly a square and the diagonal direction is also perpendicular to the highest frequency wind direction. While the diagonal is the longest straight line within the area, more WTs can be arranged along this line to reduce the mutual interference.

This article has been accepted for publication in a future issue of this journal, but has not been fully edited. Content may change prior to final publication. Citation information: DOI 10.1109/TSTE.2018.2885946, IEEE Transactions on Sustainable Energy

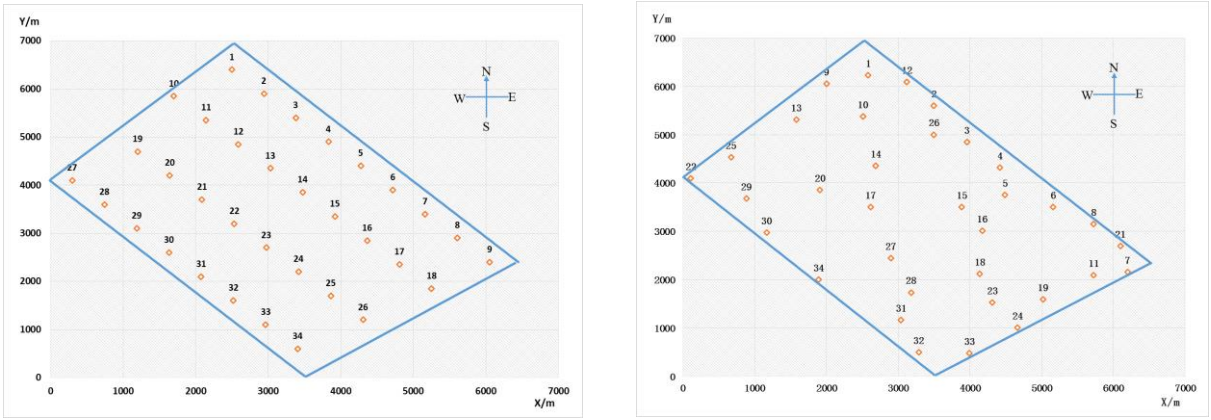

(I) (II)

Figure 8. (I)A: Traditional layout for a 34 WTs wind farm, (II)B: WT layouts of horizontal layout optimization with 34 WTs

C. *Impact of Height Selections*

Height differences of WTs in a wind farm also influence the wake effects. Joint optimizations of WT selections and layout is carried out with the nested optimization loop depicted in Fig.1 while only minimal LCOE is considered. The optimized result is shown in Fig.9(I) where the dots with different colors represent different types of WTs. Comparing Fig.9(I) with Fig.8, it can be found that: 1) Choosing and positioning WTs in a wind farm high and low will help compact the WT layout and improve the power generations. The WTs in Fig.9 (I) concentrated in the right half of the wind farm. Free space in Fig.9 (I) makes it possible to add more WTs in the wind farm. 2） In the main wind direction, WTs with smaller rotor diameters should be located upstream and WTs with larger rotor diameters prefer downstream.

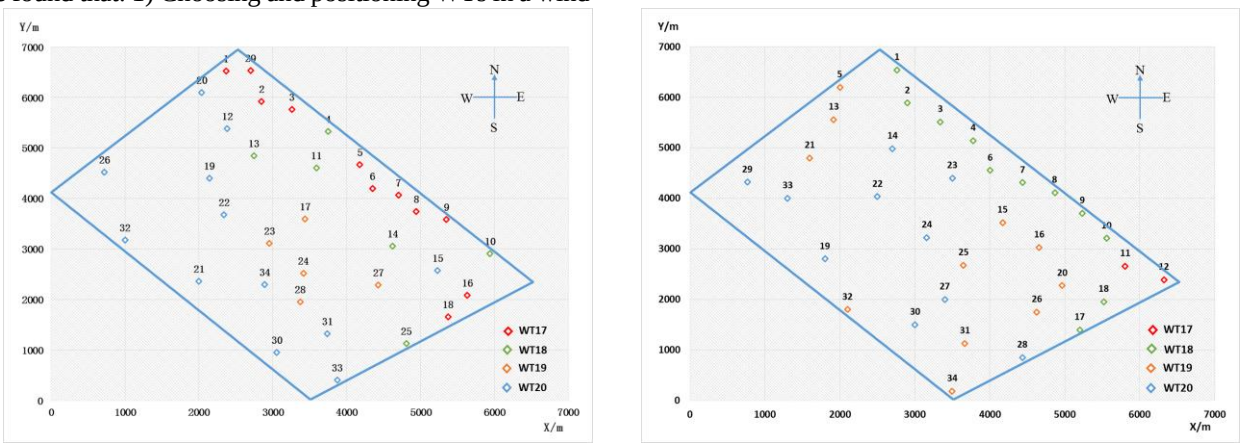

(I) (II)

Figure 9. (I) C: WT layout not considering fatigue distributions, (II)D: WT layout considering fatigue distributions

D. *3D Optimal Layout Considering Fatigue Distribution*

When fatigue damages of WTs are considered during the WTs selections and layout, there is a noticeable change in the result. The value of age reduction factor is 0.8 according to [36] while the fault fatigue value is assumed to be 0.75. The cost of prevetive maintenance and corrective replacement are assumed to be 1000$ and 200000$ every time. By running the nested loop in Fig.1 with the bi-objections of (5), 3D optimal layouts considering fatigue distribution can be obtained, as shown in Fig.9(II). Comparing the two results in Fig.9, it can be found that: 1) the smallest rotor diameter is barely selected when considering the fatigue distribution. WT 17 is with the smallest rotor diameter and there are only two WT17 in Fig.9 (II) comparing eleven in Fig.9 (I). 2) The cross-distribution is more evident when considering fatigue distribution. In Fig.9 (I), it is obvious that the WTs is lower in front and higher behind, but in Fig.9 (II), WT19 and WT20 are mixed together.

Fatigue distribution of different results is shown in Fig.10. It can be noted that: the proposed methodology helps to make the fatigue damages of the WTs much more homogeneous. The fatigue deviation decreases 84% while the values of WT fatigue vary within a small range [0.32, 0.36] in Fig.10 (II).

This article has been accepted for publication in a future issue of this journal, but has not been fully edited. Content may change prior to final publication. Citation information: DOI 10.1109/TSTE.2018.2885946, IEEE Transactions on Sustainable Energy

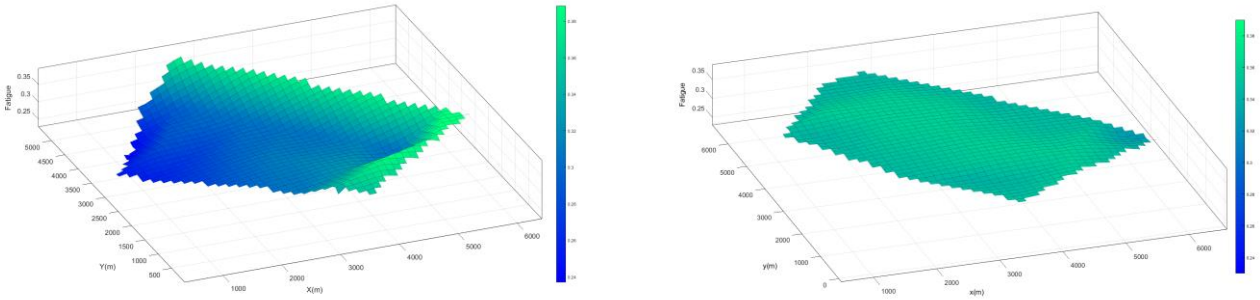

(I) (II)

Figure 10. Fatigue distribution : (I) WT fatigue distributions of A, (II) WT fatigue distributions of D

TABLE V
Results for different optimization plans

plan	Annual power generation (MWh×10^5)	Initial cost ($×$10^6$)	Corrective replacement cost ($×$10^6$)	Preventive maintenance cost ($×$10^6$)	LCC ($×$10^6$)	LCOE ($/kWh)	Fatigue standard deviation
A	4.9873	26.9812	12.4485	2.3609	86.3986	0.00866	0.0539
B	5.2716	26.9812	17.9781	2.3609	91.9282	0.00872	0.0616
C	5.3658	25.5410	12.3928	2.3609	82.5216	0.00769	0.0671
D	5.3832	25.9245	6.9937	2.3609	78.1400	0.00726	0.0086

E. Performance Comparison

Tab.V shows the results of four methods mentioned above, where A settles the WTs in wonderful arrays, B only optimizes the horizontal layout, D and C present a 3D layout with or without considering the fatigue distribution. From Tab.V, it can be found that: for the given wind farm project, the proposed methodology acquires the biggest annual power generation, the most homogeneous fatigue damages between the WTs and the lowest LCOE. The proposed methodology is improved to satisfy the multi-target requirement of wind farm planning.

Moreover, as more large WTs are applied in plan D, it increases the initial investment comparing with plan C. But, the fatigue distribution homogenization helps to decrease the corrective replacement cost significantly.

V. Conclusion

This paper presents a 3D layout optimization methodology for wind farm designs, including WT selections and WT layouts. The methodology considers the new development of low speed WT technology and builds a LCC model containing the impacts of WT fatigue to the maintenance cost. The optimization process mainly consists of a nested loop which optimizes the WT selections and WT layouts separately and repeatedly. The case analysis shows 3D layout optimization considering the fatigue distribution during WT selection and layout will help improve LCOE of the wind project as well power generations. Besides, the proposed methodology is very flexible to deal with the optimizations with different objective functions with some slight adjustments.

The case study also shows that:

1) WTs layout should take full advantages of the topography and the wind direction distributions;
2) Generally, with the same rated capacity, setting upstream WTs with smaller rotor diameters and the downstream WTs with larger ones will help to improve the power productivity and homogenizing the fatigue damages.

References

[1] Long H, Zhang Z. A Two-Echelon Wind Farm Layout Planning Model[J]. IEEE Transactions on Sustainable Energy, 2015, 6(3):863-871.

[2] Ritter M, Deckert L. Site assessment, turbine selection, and local feed-in tariffs through the wind energy index[J]. Applied Energy, 2015.

[3] Jangamshetti S H, Rau V G. Normalized power curves as a tool for identification of optimum wind turbine generator parameters[J]. IEEE Transactions on Energy Conversion, 2001, 16(3):283-288.

[4] Doddamani S S, Jangamshetti S H. Economic index for selection of wind turbine generator at a site[C]. IEEE International Conference on Sustainable Energy Technologies. IEEE, 2008:622-627.

[5] Wang L, Yeh T H, Lee W J, *et al*. Benefit Evaluation of Wind Turbine Generators in Wind Farms Using Capacity-Factor Analysis and Economic-Cost Methods[J]. IEEE Transactions on Power Systems, 2009, 24(2):692-704.

[6] Rehman S, Khan S. Fuzzy Logic Based Multi-Criteria Wind Turbine Selection Strategy—A Case Study of Qassim, Saudi Arabia[J]. Energies, 2016, 9(11):872.

[7] Yang H, Xie K, Tai H M, *et al*. Wind Farm Layout Optimization and Its Application to Power System Reliability Analysis[J]. IEEE Transactions on Power Systems, 2016, 31(3):2135-2143.

[8] Herbert-Acero J F, Franco-Acevedo J R, Valenzuela-Rendón M, *et al*. Linear Wind Farm Layout Optimization through Computational Intelligence[C]. Micai 2009: Advances in Artificial Intelligence, Mexican International Conference on Artificial Intelligence, Guanajuato, Mexico, November 9-13, 2009. Proceedings. DBLP, 2009:692-703.

[9] Sisbot S, Turgut O, Tunc M, Camdali U. Optimal positioning of wind turbines on gkeada using multi-objective genetic algorithm. Wind Energy 2009;13(4):297-306.

[10] González J S, Rodriguez A G G, Mora J C, *et al*. Optimization of wind farm turbines layout using an evolutive algorithm[J]. Renewable Energy, 2010, 35(8):1671-1681.

[11] Wu Y K, Ching-Yin L, Chen C R, *et al*. Optimization of the wind turbine layout and transmission system planning for a large-scale offshore wind farm by AI technology[C]. Industry Applications Society Meeting. IEEE, 2012:1-9.

[12] Chowdhury S, Zhang J, Messac A, *et al*. Unrestricted wind farm layout optimization (UWFLO): Investigating key factors influencing the maximum power generation[J]. Renewable Energy, 2012, 38(1):16-30.

[13] Chen Y, Li H, Jin K, *et al*. Wind farm layout optimization using genetic algorithm with different hub height wind turbines[J]. Energy Conversion & Management, 2013, 70:56-65.

[14] Abdulrahman M, Wood D. Investigating the Power-COE trade-off for wind farm layout optimization considering commercial turbine selection and hub height variation[J]. Renewable Energy, 2016, 102.

[15] Annoni, J., Gebraad, P. M., Scholbrock, A. K., Fleming, P. A., & Wingerden, J. W. V. (2016). Analysis of axial‐induction‐based wind plant control using an engineering and a high‐order wind plant model. Wind Energy, 19(6), 1135-1150.

[16] Fleming, P., Gebraad, P. M., Lee, S., Wingerden, J. W., Johnson, K., Churchfield, M., ... & Moriarty, P. (2015). Simulation comparison of wake mitigation control strategies for a two‐turbine case. Wind Energy, 18(12), 2135-2143.

[17] Fleming, P. A., Gebraad, P. M., Lee, S., van Wingerden, J. W., Johnson, K., Churchfield, M., ... & Moriarty, P. (2014). Evaluating techniques for redirecting turbine wakes using SOWFA. Renewable Energy, 70, 211-218.

[18] Su Y, Duan B, Zhu G, *et al*. Fatigue distribution and active power combined control in offshore wind farm[J]. Transactions of China Electrotechnical Society, 2015,30(22):190-198.

[19] Liu R, Research on the comprehensive optimal selection method for wind turbine generator systems[D]. Beijing: North China Electric Power Univ, 2011.

[20] Shu Z R, Li Q S, Chan P W. Investigation of offshore wind energy potential in Hong Kong based on Weibull distribution function[J]. Applied Energy, 2015, 156:362-373.

[21] Li W, Özcan E, John R. Multi-objective evolutionary algorithms and hyper-heuristics for wind farm layout optimisation[J]. Renewable Energy, 2017, 105:473-482.

[22] Zhao R, Shen W, Knudsen T, *et al*. Fatigue distribution optimization for offshore wind farms using intelligent agent control[J]. Wind Energy, 2012, 15(7):927–944.

[23] Kamal M, Rahman M M. Advances in fatigue life modeling: A review[J]. Renewable & Sustainable Energy Reviews, 2018, 82:940-949.

[24] Liu L, Yang F U, Shiwei M A, et al. Preventive Maintenance Strategy for Offshore Wind Turbine Based on Reliability and Maintenance Priority[J]. Proceedings of the Csee, 2016, 36(21).

[25] F. Gonzalez-Longatt, P. Wall, V. Terzija, Wake effect in wind farm performance: Steady-state and dynamic behavior, Renew Energy. 2012, 39 (1):329-338.

[26] Song Z, Zhang Z, Chen X. The decision model of 3-dimensional wind farm layout design [J]. Renewable Energy, 2016, 85:248-258.

[27] H. Kim, C. Singh, and A. Sprintson, "Simulation and estimation of reliability in a wind farm considering the wake-effect," IEEE Trans.Sustain. Energy, 2012,3(2): 274–282

[28] Thiringer T, Dahlberg J A. Periodic pulsations from a three-bladed wind turbine[J]. IEEE Trans on Energy Conversion, 2001, 16(2):128-133.

[29] González-Longatt F, Wall P, Terzija V. Wake effect in wind farm performance: Steady-state and dynamic behavior[J]. Renewable Energy, 2012, 39(1):329-338.

[30] Zong W G, Kim J H, Loganathan G V. A New Heuristic Optimization Algorithm: Harmony Search[J]. Simulation Transactions of the Society for Modeling & Simulation International, 2001, 76(2):60-68.

[31] Prabhu N P, Yadav P, Prasad B, *et al*. Optimal placement of off-shore wind turbines and subsequent micro-siting using Intelligently Tuned Harmony Search algorithm[C]. 2013 IEEE Power & Energy Society General Meeting. 2013:1-7.

[32] Dijk M T V, Wingerden J W V, Ashuri T, *et al*. Wind farm multi-objective wake redirection for optimizing power production and loads[J]. Energy, 2017, 121:561-569.

[33] Deb K. A fast elitist multi-objective genetic algorithm: NSGA-II[J]. IEEE Transactions on Evolutionary Computation, 2000, 6(2):182-197.

[34] Lydia M, Selvakumar A I, Kumar S S, *et al*. Advanced Algorithms for Wind Turbine Power Curve Modeling[J]. IEEE Transactions on Sustainable Energy, 2013, 4(3):827-835.

[35] Askarzadeh A. A Memory-based Genetic Algorithm for Optimization of Power Generation in a Microgrid[J]. IEEE Transactions on Sustainable Energy, 2017, PP(99):1-1.

[36] Pan L, Yan Z, Guoqin Y U, *et al*. Prediction of electrical equipment failure rate for condition-based maintenance decision-making[J]. Electric Power Automation Equipment, 2010, 30(2):91-94.

Ling-ling Huang received the B.E. from Xi'an Jiaotong University, Shanxi, China, in 2004, the M.S. degree from Zhejiang University, Zhejiang, China, in 2006, and the Ph.D. degree from Shanghai University, Shanghai, China, in 2018. Currently, she is an Associate Professor with Shanghai University of Electric Power, Shanghai, China.

Hua Tang obtained her B.E. degree and M.Sc. degree in electrical engineering from Shanghai University of Electric Power, Shanghai, China, in 2015 and 2018.
Currently, she is an engineer of State Grid Shandong Electric Power Company, Shandong, China.

Kaihua Zhang received the B.E. degree in power engineering from Shanghai University of Electric Power in1999.
Currently, he is the manager of Shanghai Green Environmental Protection Energy Co., Ltd., Shanghai, China.

Yang Fu received the Ph.D. degree in electrical engineering from Shanghai University, Shanghai, China, in 2007.
Currently, he is a Professor and Head of the Department of Electric Power Engineering at Shanghai University of Electric Power, Shanghai, China.

Yang Liu obtained B.E. degree and M.Sc. degree in electrical engineering from Shanghai University of Electric Power, Shanghai, China, in 2015 and 2017. Currently, he is working toward the Ph.D. degree in Shanghai University, Shanghai, China.